Paper 39

©Civil-Comp Press, 2012
Proceedings of the Eighth International Conference
on Engineering Computational Technology,
B.H.V. Topping, (Editor),
Civil-Comp Press, Stirlingshire, Scotland

Using Optical Flow for Analyzing the Dynamics of the Bouncing Ball System

D. Ginestar[1], J.L. Hueso[1], E. Martínez[2] and J. Riera[1]
[1]Instituto de Matemática Multidisciplinar
[2]Instituto de Matemática Pura y Aplicada
Universitat Politècnica de València, Spain

Abstract

The bouncing ball is one of the simplest dynamic systems exhibiting a great variety of behaviours ranging from periodic to chaotic motion. In this paper, we use optical flow methods to analyse the the motion of a ball bouncing under the gravity action and excited by a periodic force. We record the ball motion with a camera, obtain the optical flow associated with the ball movement and compute the spectrum of the velocities to assess the behaviour of the system. We also perform a computer simulation of the bouncing ball system and compare the results with the experimental ones.

Keywords: bouncing ball, optical flow, video analysis, dynamical systems, period doubling, numerical simulation.

1 Introduction

The bouncing ball dynamical system has been extensively studied since its introduction by Fermi [1]. It consists in a ball, moving under the gravity action, that bounces on a membrane vibrating under the action of a periodic force. The model is easy to realize in practice, allowing the comparison between the theoretical dynamics of the system, the numerical simulation and the experimental results.

In Section 2 we introduce the dynamical system modeling the bouncing ball problem, that will be used for the simulations. Section 3 reviews two kinds of optical flow algorithms for tracking the motion of the objects in a video sequence. In Section 4 we describe the experimental setup and the process of recording the video sequence to obtain the optical flow. Section 5 is devoted to compare the experimental results against the simulation results for different observed behaviors of the bouncing ball system. In the last section, we draw some conclusions and suggest lines of future work.

2 Bouncing ball models

Most of the authors use an event driven technique to derive a discrete dynamical system for the bouncing ball model [2, 3]. The key idea for these models is to compute the impact time of the ball against the membrane. At that time, the velocity of the ball instantly changes its direction and even its module if the bound is not elastic. Other authors propose a continuous time model [4] that allows a continuous change in the velocity, assuming that the ball bounces against an elastic membrane.

In general, the motion of the impact surface is assumed to be sinusoidal [5], but in some cases it is simplified to a piecewise linear, quadratic or cubic function, in order to analytically determine the collision times between the ball and the surface [6, 7, 8].

The model described below for the bouncing ball system appears in [9].

Consider an elastic ball, with coefficient of restitution ϵ, which is kept bouncing off a vertically oscillating base which vibrates sinusoidally as $S(t) = A \sin \omega t$. Between two successive collisions, the ball motion is governed by a gravitational field g. If the ball departs from the membrane at time t_i, the time of the next impact t_{i+1} is the smallest solution $t_{i+1} > t_i$ of the discrete-time dynamics map

$$A(\sin \omega t_{i+1} - \sin \omega t_i) = V_i(t_{i+1} - t_i) - \frac{1}{2} g (t_{i+1} - t_i)^2, \tag{1}$$

where V_i is the post-impact velocity, which relates to the pre-impact U_{i+1} velocity at time t_{i+1} through

$$U_{i+1} = V_i - g(t_{i+1} - t_i). \tag{2}$$

As far as the collision is partially elastic, the ball bounces back instantaneously at t_{i+1} with a relative positive velocity

$$V_{i+1} - \dot{S}(t_{i+1}) = -\epsilon[U_{i+1} - \dot{S}(t_{i+1})], \tag{3}$$

where the relative landing velocity $U_{i+1} - \dot{S}(T_{i+1})$ is always negative. Physically, the coefficient ϵ (defined as the ratio of the relative velocities before and after the collision and sometimes called restitution coefficient) gives a measure through the quantity $(1 - \epsilon^2)$ of the energy lost in the collision. Combining equations (1-3) and adimensionalizing the time and velocity variables according to $t_i \to \omega t_i \equiv \phi_i$ and $v_i \to V_i \omega / g$ gives the phase and velocity maps

$$\phi_{i+1} = \phi_i + \tau_i,$$

$$\Gamma[\sin(\phi_i + \tau_i) - \sin(\phi_i)] = v_i \tau_i - \frac{1}{2} \tau_i^2, \tag{4}$$

$$v_{i+1} = -\epsilon(v_i - \tau_i) + (1 + \epsilon)\Gamma \cos(\phi_i + \tau_i),$$

where $\Gamma = A\omega^2/g$ is the dimensionless shaking acceleration and τ_i the duration of the flight. The state variables are the phase ϕ_i and the velocity v_i after the impact. The dynamics is controlled by two parameters, Γ and ϵ. Due to the periodicity of (4) the phase ϕ can be taken modulus 2π.

Our objective is to compare the theoretical model against the measurements obtained from the experimental setup described in Section 4. The main practical difficulty is to precisely detect the times when the ball touches the membrane. In some devices found in the literature, this time is obtained placing a piezoelectric film on the vibrating surface [10] or attaching thin and light metallic wires to the ball an to a Nickel sheet deposited in the base [4]. We have tried a less invasive setup where video image processing is the main tool to obtain the data of the motion of the ball.

3 Optical flow estimation

Video tracking deals with the problem of following moving objects across a video sequence [11], and it has many applications as, for example, traffic monitoring and control [12], [13], robotic tasks, surveillance, etc.. Simple algorithms for video tracking are based on the selection of regions of interest in the first frames of the video sequence, which are associated with the moving objects and a system for estimating the movement of these regions across the sequence.

One of the main problems in the processing of image sequences is the optical flow estimation from two consecutive frames. The goal of this problem is to compute a 2D motion field that, in general, is the projection of the 3D velocities of the different objects moving in the image onto the image plane. For this computation is generally assumed that the brightness remains constant from one image to the following one. Based on this assumption many methods have proposed for the optical flow estimation [14]. Despite their differences, many of these techniques can be decomposed in three steps: 1) Prefiltering or smoothing to extract signal structure of interest, 2) The extraction of basic measurements, such as spatio-temporal derivatives or local correlations, and 3) Integration of these measurements to produce a 2D flow field.

Some of the main methods for the optical flow estimation are the so-called differential methods, where the optical flow estimation is based on computing spatial and temporal image derivatives [15]. These techniques can be classified into local (or sparse) methods, which may optimize some local energy-like expression and global (or dense) methods, which attempt to minimize a global energy functional. We will review briefly the fundamentals of one of each kind of methods. First, we will review a very popular sparse method known as the Lucas and Kanade method [16], [17] and then, the dense method proposed by Farnebäck [18].

3.1 Lucas and Kanade's algorithm

Lucas and Kanade's algorithm is a differential algorithm. This algorithm is based on what is called the optical flow restriction. To obtain this equation we denote the intensity of a frame at time t in the pixel (x, y) by $I(x, y, t)$ and assume that there exists a unknown translation (v_x, v_y), in such a way that

$$I\left(x + v_x, y + v_y, t + 1\right) = I(x, y, t) \ .$$

Using the first order approximation of Taylor expansion, we impose the restriction

$$\frac{\partial I}{\partial t}(x, y, t) + \frac{\partial I}{\partial x}(x, y, t)\, v_x + \frac{\partial I}{\partial y}(x, y, t)\, v_y = 0 \ , \tag{5}$$

which is known as the *optical flow restriction*. There are two unknown components in (5), and we have only a linear equation. Thus, further constrains are necessary to determine the components of the optical flow v_x and v_y.

Fist step in Lucas and Kanade's algorithm is to select a pixel of interest to be followed and a neighbourhood of this pixel Ω. The velocity of the pixel considered is determined minimizing the expression

$$\sum_{\vec{x}\in\Omega} W^2\left(\vec{x}\right)\left(\frac{\partial I}{\partial x}\left(\vec{x}\right)\, v_x + \frac{\partial I}{\partial y}\left(\vec{x}, t\right)\, v_y + \frac{\partial I}{\partial t}\left(\vec{x}, t\right)\right) \ , \tag{6}$$

where $W\left(\vec{x}\right)$ is a window function that weights the importance of each pixel in Ω. If n pixels are considered in Ω, the solution of this problem satisfies the system [14]

$$A^T W^2 A v = A^T W^2 b \ , \tag{7}$$

where

$$\begin{aligned} v &= \left(v_x, v_y\right)^T \ , \\ A &= \left(\vec{\nabla} I\left(\vec{x}_1, t\right), \dots , \vec{\nabla} I\left(\vec{x}_n, t\right)\right) \ , \\ W &= \operatorname{diag}\left(W\left(\vec{x}_1\right), \dots , W\left(\vec{x}_n\right)\right) \ , \\ b &= -\left(\frac{\partial I}{\partial t}\left(\vec{x}_1, t\right), \dots , \frac{\partial I}{\partial t}\left(\vec{x}_n, t\right)\right) \ . \end{aligned}$$

In typical implementations the different images are previously filtered using a Gaussian filter to attenuate temporal aliasing and quantization effects, and the partial derivatives are approximated using central finite differences formulas.

3.2 Farnebäck's algorithm

Another algorithm used to compute the optical flow is Farnebäck's algorithm [18]. This algorithm is based on the idea of polynomial expansion to approximate some neighbourhood of each pixel of the image. Here we are only interested in quadratic polynomials,

$$I\,(x) = x^T AX + b^T x + c\,. \tag{8}$$

The coefficients of this quadratic approximation are computed using a least squares fit efficiently implemented by a hierarchical scheme [19].

To compute the displacement of a given pixel x between two consecutive frames we assume that

$$I_1\,(x) = x^T A_1 X + b_1^T x + c_1$$

and

$$\begin{aligned} I_2(x) &= I_1(x+v) = (x+v)^T A_1(x+v) + b_1^T x + c_1 \\ &= x^T A_1 x + (b_1 + 2A_1 v)^T + v^T A_1 v + b_1 v + c_1 \\ &= x^T A_2 x + b_2^T x + c_2\,. \end{aligned}$$

In this way, the following relations have to be satisfied

$$A_2 = A_1 \tag{9}$$

$$b_2 = b_1 + 2A_1 v \tag{10}$$

$$c_2 = v^T A_1 v + v^T v + c_1 \tag{11}$$

and to obtain v the following system has to be solved,

$$2A_1 v = b_2 - b_1\,. \tag{12}$$

In practical implementations, the condition (9) is not satisfied and an approximate matrix

$$A = \frac{1}{2}\,(A_1 + A_2)$$

is considered and the optical flow estimation is obtained by solving the system

$$Av = \Delta b\,, \tag{13}$$

where

$$b = \frac{1}{2}\,(b_2 - b_1)\;.$$

This method can be implemented in an iterative process based in a multi-scale displacement estimation [18].

4 Experimental setup

Our system is based on recording the ball motion by means of a video camera. This allows to simplify the experimental environment.

The bouncing ball model consists in a particle bouncing on a vibrating surface. In our experiment, the particle is a table tennis ball that bounces on the membrane

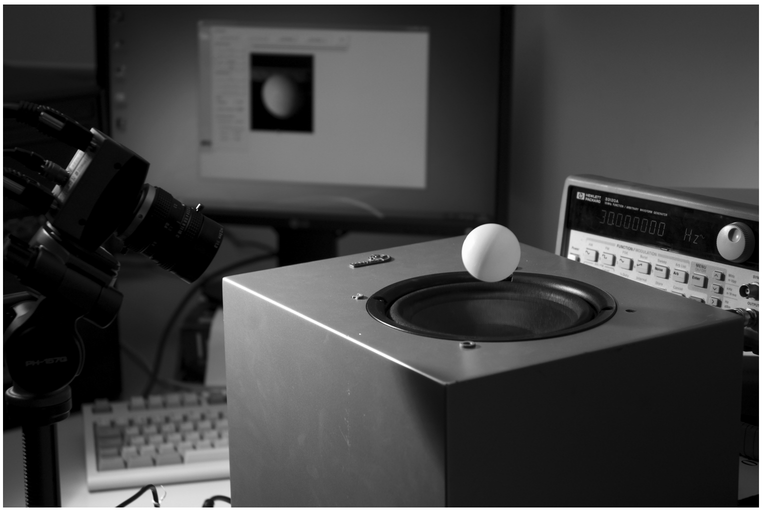

Figure 1: Experimental setup

of a loudspeaker. The loudspeaker is driven by a sinusoidal voltage with controlled amplitude. This signal is provided by a function generator and amplified by an audio amplifier to excite the vibration (see Figure 1). The vibrating frequency has been fixed to 30 Hz, using the amplitude as control parameter.

We have used a digital camera link Mikrotron Eo Sens-MC1362, that captures up to 1600 frames per second (fps). In the experiments we have registered videos at 430 fps, with frames of 256$\times$380 pixels. The camera mounts an objective Goyo Optical Inc. (focal 12.5 mm, F1.3). In order to obtain the best resolution, the camera was placed close to the trajectory (at a distance about 20 cm). This has forced us to illuminate the scene with a light source of 500W, allowing to perform the exposition with a low diaphragm aperture (f/n$\uparrow$), so reducing the minimum focusing distance. The registered images were sent to a computer running MS Windows 7, throughout a x64 xCelera-CLFull board, inserted in a PCI Expressx4 slot of the computer. The camera has been calibrated using a camera calibration toolbox for MATLAB [20].

The interest of the design is that not only allows to determine the impact time within a margin of error of 1/430 s, but also allows to track the ball along its trajectory.

The experiences are recorded in an avi file and then, the optical flow is obtained by the methods introduced in Section 3.

In the Lucas Kanade's method, we select some points in the region of interest of the first frame of the video sequence. These points are followed along the entire sequence and their trajectories are suitably filtered. Besides finding the spectra of the velocities, we can approximately draw the position of the ball along the time.

Farnebck's is a global method computes the flow all the pixels in the image. We use this algorithm to obtain the spectrum of the motion. We select a region in the frame, find the average flow of the pixels of the region in each frame and compute the fast Fourier transform of the mean flow along the sequence. The analysis of the spectrum

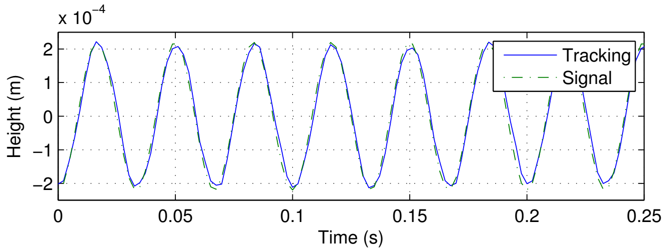

Figure 2: Membrane motion

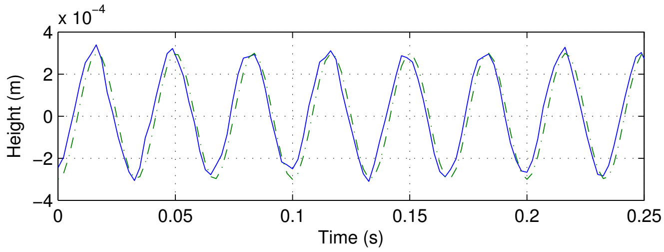

Figure 3: At 1.5 V, the ball rests in contact with the membrane

is used to check the dynamical behavior of the ball and compare it with the tracked trajectory.

5 Results

After calibrating the camera, we record the loudspeaker membrane without the ball, to determine the amplitude of the free vibration and check the accuracy of the tracking algorithm. The amplitude is also used for tuning the simulation.

As it is seen in Figure 2, the tracked motion of the membrane closely follows a sinusoid.

5.1 Driving voltage 1.5 V

Letting the ball rest on the membrane and setting the driving voltage to 1.5 V, the ball oscillates remaining in permanent contact with the membrane. Figure 3 is obtained superimposing a sinusoid vibrating at 30Hz of frequency and the amplitude of the membrane with the position the point of the ball selected for tracking. As you can see, its trajectory closely approximates the sinusoid.

Computing the spectrum of the mean flow of the sequence, we obtain a clear dominant frequency equal to the frequency of the loudspeaker (see Figure 4).

It is well known that the bouncing ball system is very sensitive to the initial conditions. With the same voltage 1.5 V, dropping the ball from a short distance to the

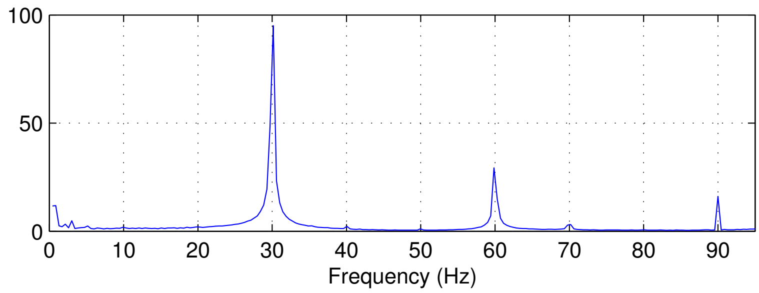

Figure 4: Simple oscillation with frequency 30 Hz at 1.5 V

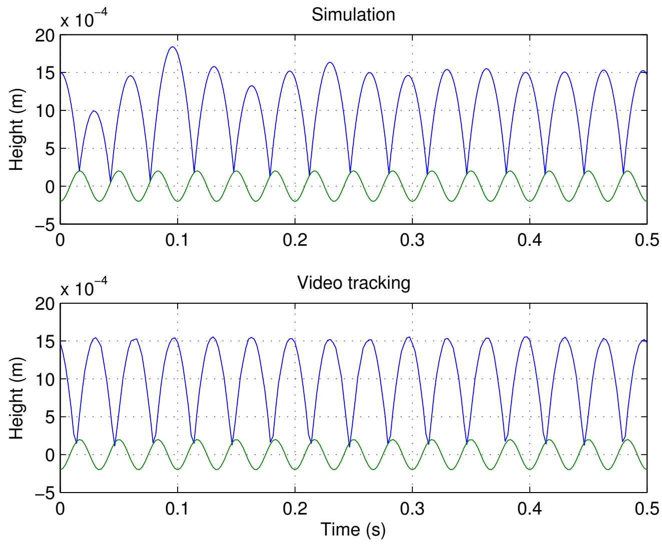

Figure 5: At 1.5 V, starting from a different position, the ball bounces at each period

membrane, it enters a periodic mode bouncing at the same frequency as the membrane. In the Figure 5, you can compare the ball motion obtained by video analysis with the corresponding simulation. The simulation shows an initial transient until the bounces become regular. This interval has not been recorded in the experiment.

Both modes of vibration are easy to distinguish in practice, because is the first case the vibration is silent whereas when the ball bounces, it produces a regular audible sound. Although the trajectories in the two modes are very different, their spectra are very similar.

5.2 Driving voltage 1.9 V

Gradually increasing the amplitude, the system looses stability and suffers a bifurcation around 1.8 V. At 1.9 V, in most cases, the dominant frequency is 15 Hz, because

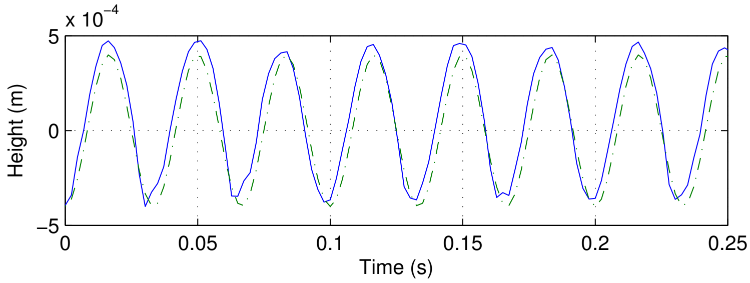

Figure 6: Chirping mode at 1.9 V

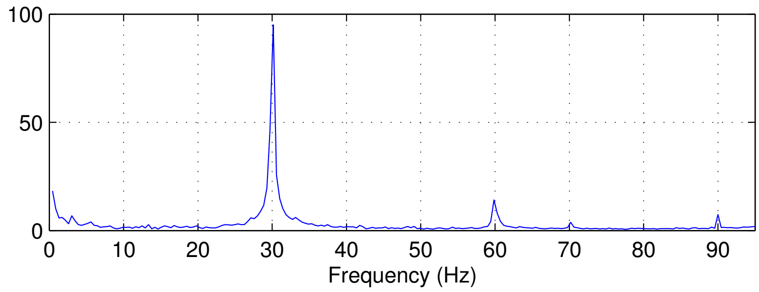

Figure 7: Spectrum of the flow in mute mode at 1.9 V

the system is in its double period mode. We have analyzed different modes of motion of the experimental system with the loudspeaker feed at this voltage.

The resting state observed at 1.5 V almost persists at 1.9 V, where the ball enters a partially mute chirping mode. Figure 6 shows the result of the flow computations on a video sequence of the ball in this mode. The irregularities are due to the fact that the period and amplitude of the bounces are close to the spatial and temporal resolution of the video recording system.

In this mode, the spectrum is slightly less smooth, but the dominant frequency is not altered by the small jumps of the ball, as it can be seen in Figure 7.

With the loudspeaker driven at the same voltage, forcing the ball to bounce, one can observe two different states of the system, both in the doubled period regime.

In the first one, the bounces are regular and span two periods each (see Figure 8).

The spectrum for this state is shown in Figure 9. The fundamental frequency has changed to 15 Hz, half the driving frequency. The spectrum smoothness suggests that the mode is quite stable for the actual value of the parameters.

In the other bifurcated state, the ball makes two different bounces in two driving periods, describing the trajectory shown in Figure 10. The tracked trajectory agrees surprisingly well with the simulated motion.

In Figure 11 there is a small peak at 7.5 Hz indication the proximity of a new period duplication.

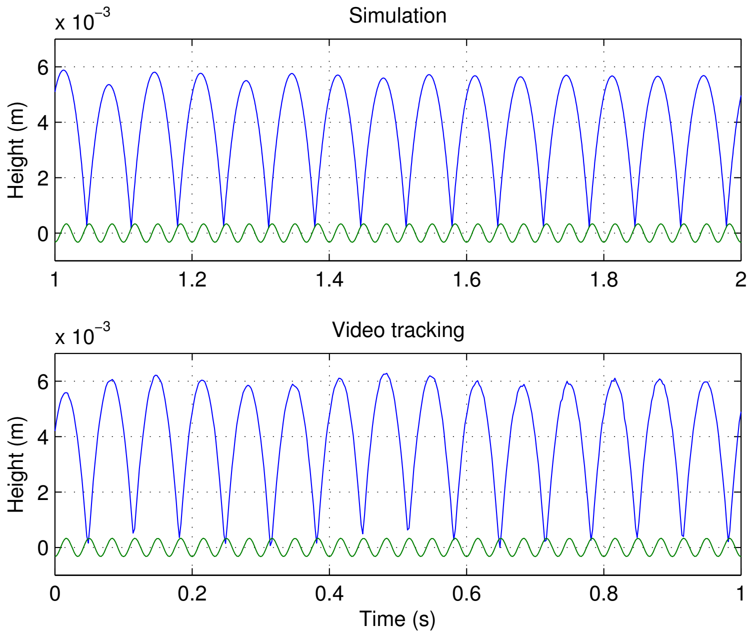

Figure 8: Equal bounces spanning 2 periods at 1.9 V

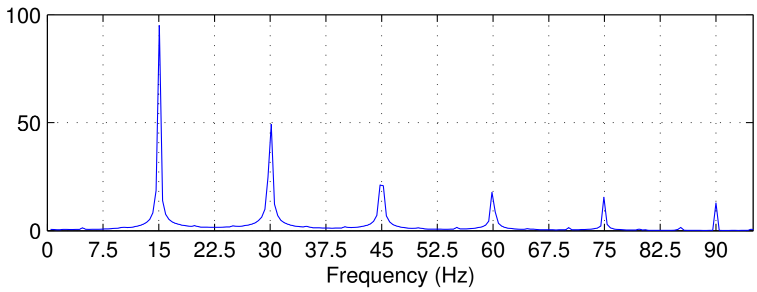

Figure 9: Doubled period at 1.9 V

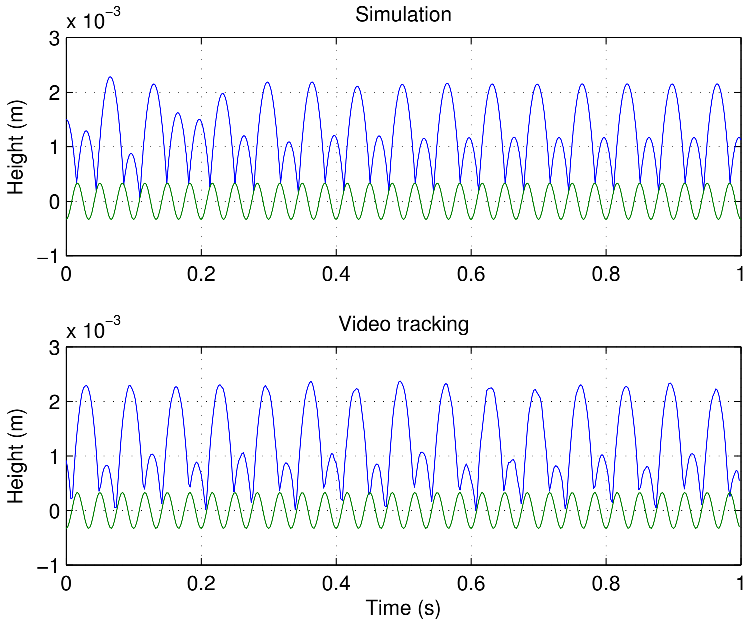

Figure 10: Different bounces spanning one period at 1.9 V

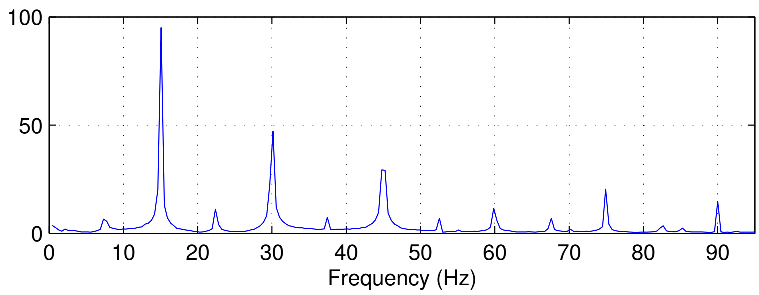

Figure 11: Doubled period, small bounces at 1.9 V. Arising of the quadruple period

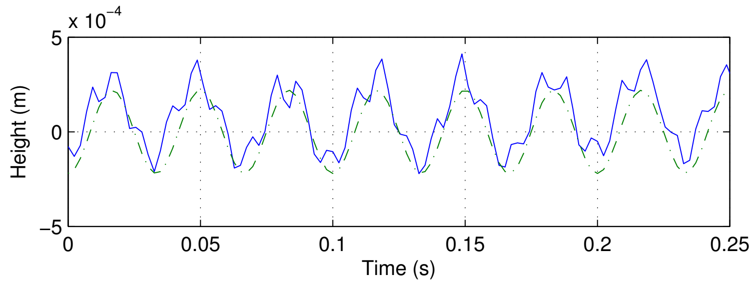

Figure 12: Chirping mode at 2.25 V

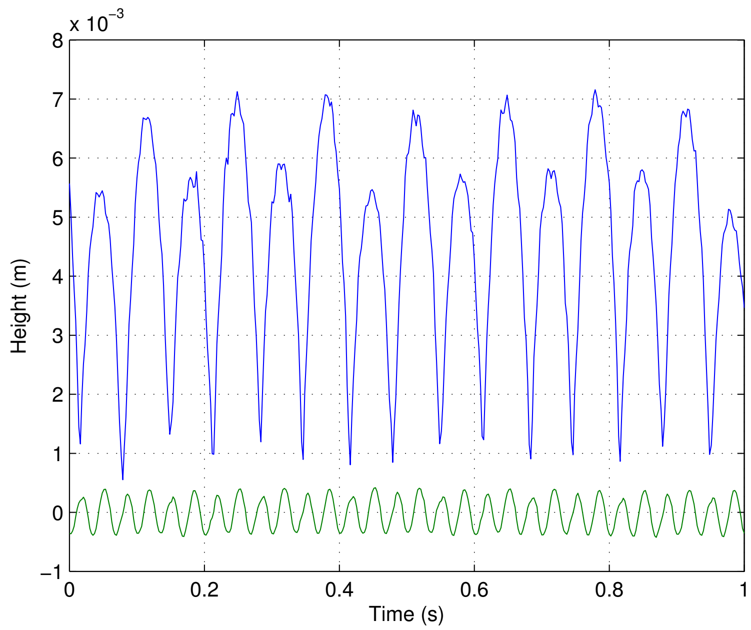

Figure 13: Tracked trajectories of ball and membrane at 2.25 V

5.3 Driving voltage 2.25 V

The double period is maintained for a range of voltage values from 1.9 V to 2.25 V, above which the motion again becomes unstable. At 2.25 V, we have recorded two different states. In one state the ball presents an audible chirping whose tracked trajectory is shown in Figure 12.

In the other state the period is quadruple ant the ball makes two different bounces spanning two periods each. In this case, we have tracked both the ball an the membrane motions. Figure 13 shows the trajectories of a point in the ball and another in the membrane. The distance between them has been adjusted in order to make the figure more clear, but the amplitude of each motion has not been scaled.

Figure 14 shows that the period has doubled, being 15 Hz the dominant frequency.

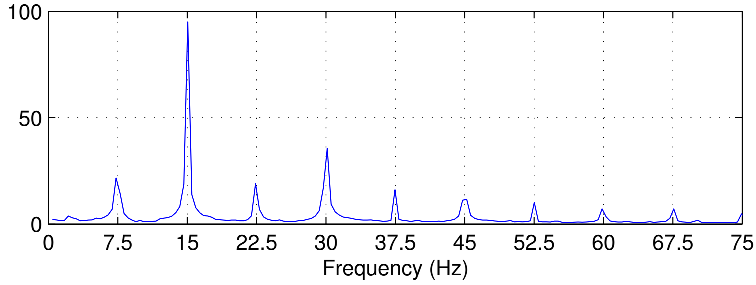

Figure 14: Doubled period at 2.25 V. Ongoing of the quadruple period

5.4 Higher driving voltages

At higher voltages, the system becomes chaotic and the ball bounces without a stable period. In the Figure 15 we have depicted the unadjusted trajectory tracked at 2.26 V and its spectrum, showing that there are no dominant frequencies.

6 Conclusions

We have described an experimental setup that allows to analyse the behaviour of the bouncing ball system using optical flow techniques. We record a video sequence of a ball bouncing on the membrane of a loudspeaker driven by a sinusoidal current, obtain the trajectory of the ball and compare it with the simulated motion derived from a discrete dynamical system that models the bouncing ball behaviour.

The optical flow allows the determination not only the impact times of the ball, but also shows the actual trajectory that the ball describes. The spectral analysis confirms that the system presents different dynamic states indicating the arising of bifurcations.

The observed states have been compared with the corresponding simulated ones, obtaining an almost perfect agreement.

In future work, different algorithms to estimate the optical flow will be applied and the obtained motions of the bouncing ball will be compared. We will also study a continuous dynamical model and its results will be compared with that of the discrete model used in this work. We will also compare the experimental results with the results of the continuous model.

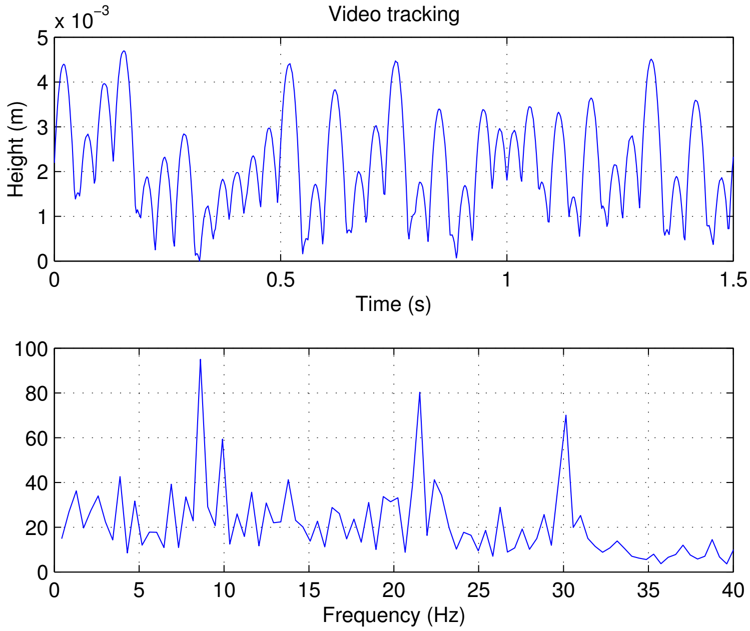

Figure 15: Chaotic motion at 2.26 v

Acknowledgments

This research has been supported by Ministerio de Ciencia e Innovación MTM2011-28636-C02-02 and by Vicerrectorado de Investigación, Universitat Politècnica de València PAID-06-2010-2285.

J. Riera is a member of the Equipo de Innovación y Calidad Educativa de la UPV, E-MACAFI.

References

[1] E. Fermi, On the Origin of the Cosmic Radiation", Physical Review, 75, 1169, 1949.

[2] J. M. Luck, A. Metha, "Bouncing Ball with a Finite Restitution: Chattering, Locking, and Chaos", Physical Review E 48(5), 1993.

[3] M. A. Naylor, P. Snchez, Michael R. Swift, "Chaotic Dynamics of an Air-damped Bouncing Ball", Physical Review E 66, 057201, 2002.

[4] B. Eichwald, M. Argentina, X. Noblin, F. Celestini, "Dynamics of a Ball Bouncing on a Vibrated Elastic Membrane", Physical Review E 82, 016203, 2010.

[5] P. Pieranski , R. Barberi, "Bouncing Ball Workbench", OWN, Poznan, 1994.

[6] A. Okninski, B. Radziszewski, "Dynamics of Impacts with a Table Moving with Piecewise Constant Velocity", Nonlinear Dynamics, 58(3), 515-523, 2009.

[7] A. Okninski, B. Radziszewski, “Simple Models of Bouncing Ball Dynamics and their Comparison”, arXiv:1006.1236v1.

[8] A. Okninski, B. Radziszewski, “An Analytical and Numerical Study of Chaotic Dynamics in a Simple Bouncing Ball Model”, Acta Mechanica Sinica, 27(1), 130-134, 2011.

[9] J. J. Barroso, M. V. Carneiro, E. E. N. Macau, “Bouncing Ball Problem: Stability of the Periodic Modes”, Physical Review, E 79, 026206, 2009.

[10] N. B. Tufillaro, A. M. Albano, “Chaotic Dynamics of a Bouncing Ball”, American Journal of Physics, 54(10), 939-944, 1986.

[11] E. Trucco, K. Plakas, “Video Tracking: A Concise Survey” IEEE Journal of Oceanic Engineering, 31(2), 520-529, 2006.

[12] R.M. Iñigo, “Application of machine Vision to Traffic Monitoring and Control”, IEEE Transactions on Vehicular Technology 38(3), 112-122, 1989.

[13] C.E. Erdem, A.M. Tekalp, B. Sankur, “Video Object Tracking with Feedback of Performance Measures”, IEEE Transactions on Circuits and Systems for Video Technology, 13(4), 310-324, 2003.

[14] J.L. Barron, D.J. Fleet, S.S. Beauchemin, “Performance of Optical Flow techniques”, International Journal of Computer Vision, 12, 1, 43-77, 1994.

[15] A. Bruhn, J. Weickert, C. Schnörr. “Lucas/Kanade Meets Horn/Schunck: Combining Local and Global Optic Flow Methods”, International Journal of Computer Vision, 61, 3, 211-321, 2005.

[16] B. Lucas, T. Kanade, “An Iterative Image Registration Technique with Applications to Stereo Vision”, Proceedings of the Seventh International Joint Conference on Artificial Intelligence, Vancouver, Canada, 674-679, 1981.

[17] S. Baker, I. Mattews, “Lucas-Kanade 20 Years On: A Unifying Framework”, International Journal of Computer Vision, 56, 3, 221-255, 2004.

[18] G. Farnebäck, “Two-Frame Motion Estimation Based on Polynomial Expansion”, Lecture Notes in Computer Science, 2749, 363-370, 2003.

[19] G. Farnebäck, “Polynomial Expansion for Orientation and Motion Estimation”, PhD thesis, Linköping University, Sweden, SE-581 83, Dissertation No 790, ISBN 91-7373-475-6, 2002.

[20] J.Y. Bouguet, “Camera Calibration Toolbox for Matlab”, http://www.vision.caltech.edu/bouguetj/index.html , Retrieved april, 2012.